

A Preliminary Study to discriminate aMCI and dMCI with Multiple Clinical Neuroimaging Characteristics Using Random Forests Classifier

Shih-Ting Yang¹, Jiann-Der Lee^{1,2,3}, Hong-Yuan Tzou¹ and Wen-Chuin Hsu^{4,5}

ABSTRACT

In this study, a classification scheme, using the features from resting-state functional MRI (rs-fMRI) and voxel-based morphometry (VBM), was proposed to discriminate two subtypes of mild cognitive impairment (MCI): amnesic MCI (aMCI) subtypes and dys executive MCI (dMCI) subtypes. More specifically, this scheme employed random forests (RF) algorithm to classify three study groups i.e., healthy controls (NC), aMCI, and dMCI. With the hybrid framework, the classification accuracy achieves 77.42% (AUC=0.8101) between aMCI and NC, and 82.14% (AUC=0.8473) between dMCI and NC. If comparing two MCI subtypes against each other, the accuracy can reach 79.57% (AUC=0.8410). The preliminary results suggest that pattern matching using the features from multiple modalities can achieve a clinically relevant accuracy for the a priori diagnosis in MCI subtypes.

Keywords

Mild cognitive impairment, Resting state functional magnetic resonance imaging, Functional connectivity, Voxel-based morphometry, Random forests

Introduction

As reported in [1-4], Alzheimer's disease (AD) is a progressively neuro-degenerative disorder characterized by leading to deficit of cognitive functions, such as memory loss and cognitive degeneration, and behavioral impairment, resulting in declining quality of daily life. Since AD is irreversible and there is no cure, current treatment focuses on lessening its symptoms. Therefore, how to diagnose AD accurately in early stage has become increasingly significant.

Mild cognitive impairment (MCI) is considered

as a transitional stage between normal aging and dementia [5]. Early researches focused on MCI patients with predominant memory impairment and the risk for progression to AD [6]. However, recent studies show the prodromal stage of several neuro-degenerative disorders may begin with non-amnesic cognitive decline (e.g. dysexecutive, language, visuospatial) [7]. Hence this degenerative brain disorder can be divided into two categories: amnesic MCI (aMCI) subtypes and dysexecutive MCI (dMCI) subgroups [5]. In Yaffe's research [8], it is observed that dMCI subtypes were less likely

¹Department of Electrical Engineering, Chang Gung University, Taoyuan, Taiwan 333

²Department of Neurosurgery, Chang Gung Memorial Hospital at Linkou, Taoyuan, Taiwan 333

³Department of Electrical Engineering, Ming Chi University of Technology, New Taipei City, Taiwan 24301

⁴Department of Neurology, Chang Gung Memorial Hospital Linkou Medical Center and College of Medicine, Chang Gung University, Taoyuan, Taiwan 333

⁵Dementia Center, Chang Gung Memorial Hospital, Taoyuan, Taiwan 333

[†]Author for correspondence: Jiann-Der Lee, Department of Electrical Engineering, Chang Gung University, Taoyuan, Taiwan 333; Department of Neurosurgery, Chang Gung Memorial Hospital at Linkou, Taoyuan, Taiwan 333; Department of Electrical Engineering, Ming Chi University of Technology, New Taipei City, Taiwan 24301. Phone: 03-2118800, Ext: 5316, email: jdlee@mail.cgu.edu.tw

to convert to AD but had higher rates of death over five years than aMCI subgroups because these subgroups will have different etiologies and outcomes. In Huey's report [9], patients with dMCI were more likely to experience stroke, detected via MRI than patients with aMCI. Additionally, Chao's study [10] found that aMCI patients would show perfusion abnormalities in the medial parietal cortex, and dMCI patients would show perfusion abnormalities in the frontal cortex. It is, therefore, important to subdivide MCI groups to improve the effects of clinical treatment.

Generally speaking, functional MRI (fMRI) is a neuroimaging technique that is presumed to directly link specific cognitive activity to neurophysiological changes, such as functional cerebral hemodynamics. fMRI studies, based on blood oxygen level dependent (BOLD) contrast, have shown that cognitively intact older individuals that demonstrate a greater degree of activation in many literatures [11-15]. Therefore, it appears that fMRI activation might be predictive of future cognitive decline during the prodromal stages of AD and MCI. The resting state functional MRI (rs-fMRI) of the brain is measured by spontaneous low frequency fluctuations in BOLD signal patterns across anatomical regions. A correlation of these low frequency fluctuating time courses, generated by their spontaneous activity, can be used to establish the degree of functional connectivity between regions. Examination of rs-fMRI connectivity might be an even more useful technique for observing the initial functionally related changes that occur in AD and prior to behavioral manifestations [16-17]. Moreover, interest in rs-fMRI has steadily grown since its inception. Resting state functional connectivity has been shown to exist in a number of brain networks [18-19], has been revealed with data-driven analysis approaches [20-22], and has been found to be consistent across subjects [23]. These fluctuations are consistent with the concept of functional connectivity (FC) defined by Friston *et al.* [24] and are thought to represent alterations in blood flow and oxygenation caused by spontaneous neuronal activity [25]. Several recent studies have shown changes in low-frequency correlations for patients in pathological states, inclusive of AD [26,27]. Therefore, in this study, rs-fMRI can reflect spontaneous low-frequency fluctuations (< 0.1 Hz) in BOLD signal and then be used

to investigate the functional architecture of the brain by measuring FC [28].

Voxel-based morphometry (VBM) [29-32] is an automated technique that uses statistics to identify differences in brain anatomy between groups of subjects. Thus, it can be employed to infer the presence of atrophy or, less commonly, tissue expansion in subjects with disease. The technique typically uses T1-weighted volumetric MRI scans and essentially performs statistical tests across all voxels in the image to identify volume differences between groups. For example, to identify differences in patterns of regional anatomy between groups of subjects, a series of *t* tests are performed at every voxel in the image. Regression analyses are then performed across voxels to assess neuroanatomical correlates of cognitive or behavioral deficits. The technique has been applied to a number of different disorders, contributing to the understanding of how the brain changes in these disorders and how brain changes relate to characteristic clinical features. Therefore, in this study, we also employ VBM to discriminate the abnormal changes between aMCI and dMCI.

In previous studies described as above, whether rs-fMRI or VBM, can both display the differences of region variances and region positions of brain between different ethnic groups. One thing is worth noting that two methods are analyzed and compared in specific data using the statistical approach. In other words, variances of results displayed in these specific cases may not be applicable in all clinical data. To assess the reliability of results, we adopt random forests (RF) [33] for classification. Basically, RF is an ensemble classifier consisting of many decision trees, where the final predicted class for a test example is the mode of the predictions of all individual trees.

In summary, the objectives of this study are as follows:

- a) Examining the dysfunctions of brain regions and abnormal changes of FC in different MCI subtypes and normal individuals using rs-fMRI;
- b) Evaluating brain atrophy patterns in different MCI subtypes and normal individuals using VBM;
- c) Assessing the performance of combining these features (rs-fMRI / VBM / rs-fMRI + VBM) with RF to classify different study groups.

Methods

■ **Study population**

All MR image data adopted in this study were provided by Chang Gung Memorial Hospital, Lin-Kou, Taiwan. The degree of clinical severity for each participant was evaluated by experienced clinicians conducted independent semi-structured interviews which included a set of questions regarding the functional status of the participant, along with a standardized neurologic, psychiatric, and health examination. This interview generates an overall Clinical Dementia Rating (CDR) and Mini Mental State Examination (MMSE) score. The whole dataset consists of three groups comprising normal controls (NCs), aMCI and dMCI: 48 NCs (M/F=26/22), 40 patients with aMCI (M/F=21/19), and 29 patients with dMCI (M/F=14/15). All study subjects gave written informed consent. Demographic information is provided in **Table 1**.

■ **MRI data acquisition**

The whole-brain structural and functional MRI scans were obtained by a 3-Tesla MR scanner (Magnetom Trio with TIM system, Siemens, Erlangen, Germany). T1-weighted images were acquired by magnetization-prepared 180 degrees radio-frequency pulses and rapid gradient-echo (T1-MPRAGE) series. The following imaging parameters were used: repetition time (TR)=2000 ms, echo time (TE)=4.16 ms, and flip angle=9 degrees. The results were represented as a 224 × 256 matrix, and slice thickness=1 mm in 160 slices.

BOLD rs-fMRI data were acquired in four runs lasting four minutes each by means T2*-weighted echo planar imaging (EPI) free induction decay (FID) sequences applying the following parameters: TR=1671 ms, TE=35 ms, matrix size=64×64, field of view (FOV)=256 mm, in-plane voxel size=4 × 4 mm, flip angle=75 degrees, slice thickness=4mm and no gap. Functional volumes consisted of 30 trans-axial slices. All subjects were asked to relax, stay awake, and don't need to do anything [34].

■ **Diagnostic criteria**

The clinical work-up included a thorough medical history, physical examination, and neuropsychological testing. The following four key cognitive domains were assessed: memory, executive function, language, and visuospatial

Table 1: Demographic data and cognitive scores.

Group	Normal control	aMCI	dMCI
Individuals (Male/Female)	48 (26/22)	40 (21/19)	29 (14/15)
Mean age (yrs)	64.36 ± 6.26	67.47 ± 8.53	65.62 ± 5.47
Education time (yrs)	9.54 ± 4.17	7.12 ± 4.93	9.87 ± 4.58
MMSE scores	28.72 ± 1.03	24.93 ± 4.25	27.87 ± 0.99
CDR scores	0.00± 0.00	0.50± 0.00	0.19± 0.15

skills. All subjects were screened for the presence of depressive symptoms using either the Hamilton Depression Rating Scale (NC) or the Cornell scale for depression in dementia (aMCI and dMCI). Patients with depression were excluded.

The mini mental state examination (MMSE) and clinical dementia rating (CDR) were used to quantify the severity of symptoms of dementia. aMCI and dMCI patients were diagnosed after an extensive clinical evaluation. The clinical phenotype of MCI was determined according to the criteria by Petersens *et al.* [5]. Cognitively healthy controls were free of cognitive impairment as judged by clinical assessment, neuropsychological testing, and clinical dementia rating.

■ **Pre-processing of structural and functional MR images**

In order to compare the data from several scans and / or research subjects, all the brain images have to be in the same 3D space. In this study, spatial normalization was performed using statistical parametric mapping software (SPM8) [35]. Spatial normalization is a procedure to register a MRI data set to a standard coordinate system [36]. Therefore, each voxel is thus comparable with the other registered MRI or a reference template. The normalization herein was performed by using a 12-parameter affine transform and a Bayesian framework to a T1-weighted MRI template, provided by ICBM, NIH P-20 project [37].

In addition to spatial normalization, EPI volumes were also processed using SPM8 including steps with an order of slice timing correction (the first 10 volumes of each functional time series were excluded from analysis in advance), head motion correction, and spatial smoothing with 8 mm isotropic full-width-at-half-maximum Gaussian kernel.

■ **Image analysis of rs-fMRI**

rs-fMRI analysis was performed and the FC was identified using Resting-state fMRI data analysis Toolkit (REST) [38] in this study. In order to

obtain required FC, some possible spurious variances (e.g. signals from a region centered in cerebrospinal fluid and white matter, or global signal averaged over whole brain) must be removed using linear regression. Power spectrum of low-frequency signals was collected using temporally band-pass filter (0.01 - 0.08 Hz). To get FC maps, Pearson's correlation coefficient was calculated between residual time series of every seed point in a hemisphere and those of every vertex in the other (target) hemisphere, as shown in Eq. (1).

$$r = \frac{\sum_{i=1}^n (X_i - \bar{X})(Y_i - \bar{Y})}{\sqrt{\sum_{i=1}^n (X_i - \bar{X})^2} \sqrt{\sum_{i=1}^n (Y_i - \bar{Y})^2}} \quad (1)$$

where r is Pearson correlation coefficient, \bar{X} and \bar{Y} are the mean values of time course X and Y , respectively. Seed point is predefined centered at a coordinate [0, -56, 30] within posterior cingulate cortex (PCC) in REST software. Individual Pearson correlation r -maps were converted to normally distributed Z -maps by using Fisher's Z transformation, as shown in Eq. (2). Finally, all Fisher's Z -maps were entered into a two-tailed one-sample t -test to detect the regions showing significant FC with PCC.

$$Z = \frac{1}{2} [\ln(1+r) - \ln(1-r)] \quad (2)$$

■ Image analysis of VBM

In general, VBM used statistic algorithm to identify differences in brain anatomy between different groups of subjects, which in turn can be used to infer the presence of atrophy or tissue expansion in subjects with disease. Here, we adopted VBM to calculate differences in patterns of regional atrophy between groups of NCs, aMCI, and dMCI.

In order to observe the atrophy in gray matter of brain, all T1-weighted images were segmented into gray matter (GM), white matter (WM), and cerebrospinal fluid (CSF) based on the intensity of the image as well as prior probability maps which indicate the likelihood of finding a given tissue class at a given location. General linear model and the theory of Gaussian random fields were adopted in VBM to find the significance in statistics, as shown in Eq. (3).

$$F_{\text{discrepancy}} = \frac{A}{B} \quad (3)$$

$$A = \frac{\Delta R^2}{m}, \quad B = \frac{R^2}{n - m - o - 1}$$

where n is number of subjects, m is number of voxelwise covariates, o is number of non-voxelwise covariates, ΔR^2 is the difference in the

proportion of variance, and R^2 is proportion of total variance.

■ Specific volume features extraction

In analytic steps of rs-fMRI and VBM, we extract significant differences in brain regions of NCs, aMCI, and dMCI. These results reflect the degree of difference between different ethnic groups in a specific area. In order to increase the discriminative features used in the subsequent classification, FreeSurfer [39] was adopted to segment regions that are equivalent to rs-fMRI and VBM automatically.

■ Random forests

As shown in Figure 1, Random Forests (RF) [34] is a popular classifier consisting of a collection of tree-structured classifiers $R(x; \theta_k)$, $k=1, 2, 3, \dots$, where the θ_k are independent identically distributed random vectors and each tree casts a unit vote for the most popular class at input x . The specialty of this combination is that each decision tree is built from a random vector of parameters. Basically, RF algorithm grows many decision trees. To classify a new object from an input vector, the input vector is run down each of the trees in the forest. Each tree gives a classification and each tree votes for the class. In RF, it was shown that the forest error rate depends on two things: correlation and strength. Increasing the correlation increases the forest error rate. On the contrary, increasing the strength of the individual trees decreases the forest error rate. The training set for each individual tree in a random forest is constructed by sampling N examples at random with replacement from the N available examples in the dataset. This is known as bootstrap sampling, and bagging describes the aggregation of predictions from the resulting collection of trees. As a result of the bootstrap sampling procedure, approximately one third of the available N examples are not present in the training set of each tree. These are referred to as the out-of-bag data of the tree, for which internal test predictions can be made. By aggregating the predictions of the out-of-bag data across all trees, an internal estimate of the generalization error of the random forest can be determined.

More specifically, at each node in a tree, $d \ll D$ features are randomly selected, and the node is partitioned using the best possible binary split. RF error rate depends on both the correlation between trees ρ and the strength of the collection

of trees s [40], such that an upper bound for the generalization error is given by $\bar{\rho}(1-s^2)/s^2$. A reduction in the selected value of d results in a corresponding reduction in both $\bar{\rho}$ and s . optimal range for d therefore exists, which is generally quite wide. The recommended default value for most applications is $d=\sqrt{D}$ [32].

A parent node n_p is partitioned into child nodes n_l and n_r according to an impurity criterion which aims to maximize the homogeneity of the child nodes with respect to the parent node. Impurity is assessed using Gini index I_G , which measures the likelihood that an example would be incorrectly labeled if it were randomly classified according to the distribution of labels within the node. For two classes C_1 and C_2 , Gini index of a node n may be defined as Eq. (4)

$$I_G(n) = 1 - \sum_{k=1}^2 p_k^2 \quad (4)$$

where p_k is the relative proportion of examples belonging to class K present in the node n . Therefore, the range of Gini index is from minimum of zero to maximum value of $(1 - 1 / K)$. A value of zero indicates that the node contains only examples belonging to a single class, and the maximum value indicates that the node contains examples belonging to both classes in equal proportions. The best possible binary split is the one which maximizes the improvement in Gini index $\Delta I_G(n_p) = I_G(n_p) - p_l I_G(n_l) - p_r I_G(n_r)$. Where p_l and p_r are the proportions of examples in node n_p that are assigned to child nodes n_l and n_r , respectively. The Gini index can also be used to assess the relative importance of the various features for classification. A measure of the importance of an individual feature may be computed by summing the decreases in Gini index ΔI_G occurring at all nodes in the forest which are partitioned based on that feature.

In this study, we divided all participants into two classes randomly: a) feature searching class, and b) classified (training-and-test) class. We used the cluster of feature searching to obtain statistical differences of rs-fMRI and VBM between three groups. 30 NCs (M/F=17/13), 30 patients with aMCI (M/F=16/14), and 15 patients with dMCI (M/F=7/8) are included in this cluster. The rest of data are belonging to the cluster of classification. In the experiment, leave-one-out cross-validation (LOOCV) is adopted to estimate dependable generalization error. LOOCV involves using a single observation from the original sample

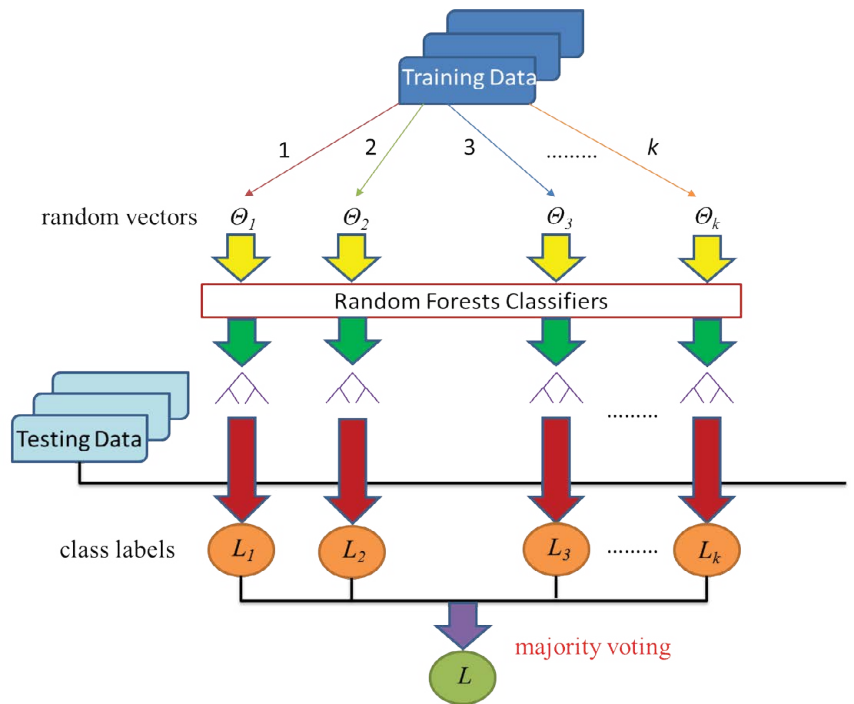


Figure 1: The operating schema of random forests.

as the validation data, and the remaining observations as the training data. No random factors which will affect the experimental data, to ensure that the experiment can be replicated.

Results and Discussion

■ Evaluation of rs-fMRI and VBM

aMCI vs. NCs: **Figure 2** illustrates the differences of FC and VBM between NCs and aMCI. **Table 2** provides a list of the brain regions that have significant discrepancies, where +/- indicates the regions of increased / decreased FC or VBM in aMCI compared with NCs.

dMCI vs. NCs: **Figure 3** illustrates the differences of FC and VBM between NCs and dMCI. **Table 3** is the list of the brain regions that have significant discrepancies, where +/- indicates the regions of increased / decreased FC or VBM in dMCI compared with NCs.

aMCI vs. dMCI: **Figure 4** illustrates the differences of FC and VBM between aMCI and dMCI. **Table 4** provides a list of the brain regions that have significant discrepancies, where +/- indicates the regions of increased / decreased FC or VBM in aMCI compared with dMCI.

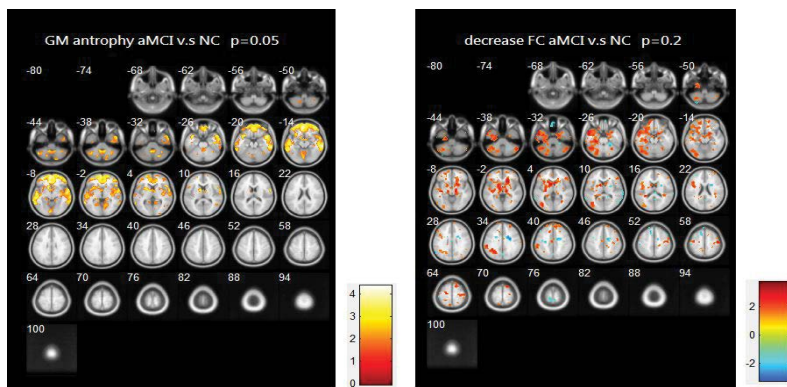


Figure 2: (a) FC differences between aMCI and NCs, (b) VBM differences between aMCI and NCs.

Table 2: List of significant differences of brain regions (aMCI vs. NCs).

Region	Methods	
	rs-fMRI	VBM
+	Frontal Gyrus - Inferior - Superior	Frontal Gyrus - Medial - Inferior - Superior - Middle
	Temporal Gyrus - Superior - Middle	Temporal Gyrus - Superior - Middle
	Putamen	Putamen
	Hypothalamus	Hypothalamus
	Declive	Declive
	Caudate	Parahippocampa Gyrus
	-	Postcentral Gyrus

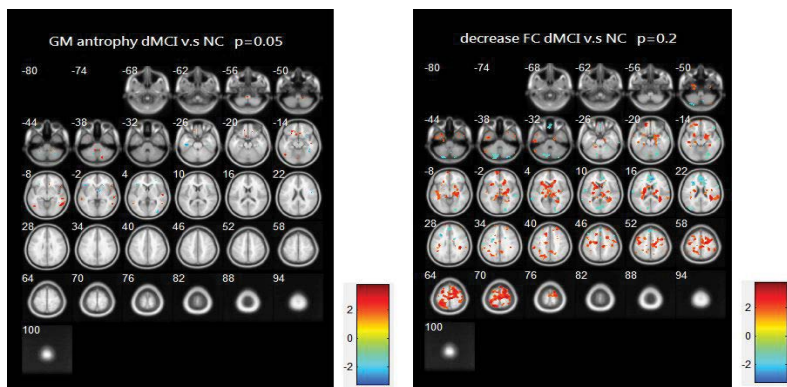


Figure 3: (a) FC differences between dMCI and NCs, (b) VBM differences between dMCI and NCs.

■ **Evaluation of classification**

Classified accuracy (ACC), sensitivity (SEN), specificity (SPEC), and area under curve (AUC) were evaluated in the three test sets resulting from the LOOCV strategy as described above. The definition of accuracy, sensitivity and

specificity are expressed in Eq. (5) – Eq. (7), where TP=true positive, TN=true negative, FP=false positive, and FN=false negative. Here, we extract the brain regions that have statistically significant differences using rs-fMRI and VBM algorithms. Next, we adopt significant regions’ Z-scores and volumes corresponding to regions segmented by FreeSurfer as features, and then assessing the performance of combining these features (rs-fMRI / VBM / rs-fMRI + VBM) with random forest decision tree (RF) to classify different testing data. **Table 5** is the list of all features we adopted and trained in this study, and the classification results for different types of features are summarized in **Table 6**.

$$Accuracy (ACC) = (TP + TN) / (TP + TN + FP + FN) \quad (5)$$

$$Sensitivity \text{ or true positive rate } (TPR) = TP / (TP + FN) \quad (6)$$

$$Specificity \text{ or True Negative Rate } (TNR) = TN / (FP + TN) \quad (7)$$

Discussion

The resting brain activations in the between-group comparisons using REST toolkit are presented in **Table 2-4** and **Figures 2-4**. From experimental results, it is observed that the trend for brain activation in inferior frontal gyri, middle frontal gyri, and temporal gyri were detected, where NCs showed significant increasing. In comparisons of aMCI-dMCI pairs, dMCI patients also displayed same trend for activation in frontal gyri. Because dMCI patients belong to executive function impairments, this result is reasonable that FC is higher than aMCI group. The frontal lobe contains most of the dopamine-sensitive neurons in the cerebral cortex, is associated with working memory tasks and short-term memory tasks. This result also indirectly illustrates that aMCI patients reveal some problems in memory function comparing with NCs and dMCI patients. The dMCI patients did not reveal greater activations in any brain areas when compared to aMCI, but there was a significant decline in Brodmann area 6. Brodmann area 6 is composed of premotor cortex and supplementary motor area (SMA) that is believed to play a role in the planning of complex, coordinated movements. Trend for stronger activation was also detected in postcentral and middle occipital gyri (aMCI vs. NCs). aMCI patients also showed poor activation

in hypothalamus, putamen, and caudate, which is also associated memory function. Moreover, dMCI subjects also revealed lower activation in postcentral gyri and insula because they involve in primary motor areas.

Statistical significance of VBM structural results in the between-group comparisons are also presented in **Table 2-4** and **Figures 2-4**. Compared with NCs, aMCI subjects revealed a significant GM volume reduction in frontal gyri, parahippocampa gyri, and related regions in hypothalamus and putamen that controlled memory function. There was a trend towards more atrophy in frontal as well as parietal temporal cortices in MCI subtypes. When compared to dMCI subjects, aMCI patients showed a trend for GM volume loss in temporal cortex. dMCI subjects revealed GM volume loss in lingual gyri. The lingual gyrus is a structure in the visual cortex that plays an important role in the identification and recognition of words. Atrophy in lingual gyri maybe cause difficulty in reading comprehension indirectly (dysexecutive). In comparisons of dMCI-NCs pairs, VBM results displayed GM volume reduction in parahippocampa gyri of NCs. We thought it is mainly due to dMCI patients belong to executive function impairments, not memory function impairments. So atrophy in parahippocampa gyri may not occur.

By combining rs-fMRI (Z-score), VBM (F-score), and volumetric features, the classification accuracy of RF reached to 77.42% (area under curve, AUC=0.8101) and 82.14% (AUC=0.8473) in patients with aMCI and dMCI, respectively. If comparing two MCI subtypes against each other, the accuracy can reach 79.57% (AUC=0.8410). According to the results, combining RF with multi-modality predictors would achieve the best accuracy of classification. Moreover, if just consider ACC and SEN, the identified ability of functional features seems to be better than volume features no matter comparative aMCI and NCs, dMCI and NCs, or aMCI and dMCI. This result also may be explained that the pattern of aMCI or dMCI at early stages followed by a loss of brain activation as cognitive impairment worsens is similar to the pattern seen in individuals with Alzheimer dementia, and functional features have the potential to be detected at early stage before patient's brain starts apparent atrophy.

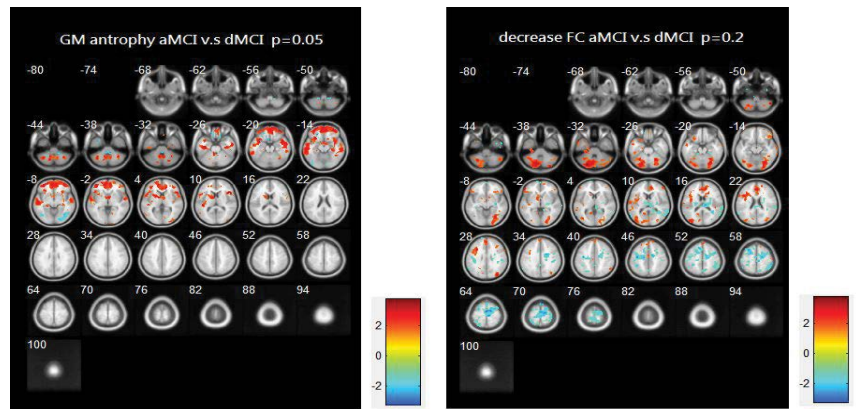


Figure 4: (a) FC differences between aMCI and dMCI, (b) VBM differences between aMCI and dMCI.

Table 3: List of significant differences of brain regions (dMCI vs. NCs).

Region	Methods	
	rs-fMRI	VBM
+	Frontal Gyrus - Medial - Superior - Middle	Frontal Gyrus - Inferior
	Temporal Gyrus - Superior	Temporal Gyrus - Superior - Middle
	Putamen	
	Postcentral Gyrus	
	Insula	
	Caudate	
-		Parahippocampa Gyrus

Table 4: List of significant differences of brain regions (aMCI vs. dMCI).

Region	Methods	
	rs-fMRI	VBM
+	Frontal Gyrus - Medial - Inferior	Frontal Gyrus - Medial - Inferior - Superior - Middle
		Temporal Gyrus - Superior - Middle
	Declive	
-	Middle Frontal Gyrus Brodman area 6	Lingual Gyrus

Conclusion

In this study, we design a classification framework for image-aided diagnosis in early prodromal Alzheimer’s disease by using rs-fMRI and VBM. Based on the experimental results, it is clear that combining rs-fMRI, VBM, and specific volumetric features achieve better MCI classification performance than only individual features used. It is because

Table 5: List of all training features.

Features		
rs-fMRI (Z-score)	VBM (F-score)	Volume of tissue
Frontal Gyrus - Medial - Inferior - Superior - Middle	Frontal Gyrus - Medial - Inferior - Superior - Middle	Frontal Gyrus - Medial - Inferior - Superior - Middle
Temporal Gyrus - Superior - Middle	Temporal Gyrus - Superior - Middle	Temporal Gyrus - Superior - Middle
Putamen	Putamen	Putamen
Hypothalamus	Hypothalamus	Hypothalamus
Declive	Declive	Declive
Caudate	Parahippocampa Gyrus	Caudate
Postcentral Gyrus	Lingual Gyrus	Parahippocampa Gyrus
Insula		Postcentral Gyrus
		Lingual Gyrus
		Insula

Table 6: Classification results.

Proportion	rs-fMRI	VBM	Volumes	Mixed
aMCI from NCs				
ACC (%)	72.58	67.86	65.16	77.42
SEN (%)	71.75	70.37	69.84	82.31
SPEC (%)	69.35	73.05	70.61	72.00
AUC	0.7142	0.7164	0.6898	0.8101
dMCI from NCs				
ACC (%)	78.57	64.27	53.57	82.14
SEN (%)	79.62	68.02	57.69	85.19
SPEC (%)	81.71	67.31	69.05	87.80
AUC	0.8092	0.6714	0.5649	0.8473
aMCI from dMCI				
ACC (%)	77.78	62.71	62.90	79.57
SEN (%)	75.00	65.38	69.70	83.96
SPEC (%)	80.93	70.81	61.02	88.24
AUC	0.7931	0.6493	0.6466	0.8410

multiple imaging modalities can provide complementary information to increase the classification accuracy. For the future work, we will increase the size of the dataset to support the outcome of this experiment. In addition, according to the classification results, MCI is apparently similar between normal aging and dementia. Therefore, more features should be investigated to improve the classification performance. For example, DTI can be used to assess the fiber integrity. Electroencephalography (EEG) and cerebrospinal fluid biomarkers can also be added to improve classified accuracy.

This information will help us to improve the outcome of diagnosing neurodegenerative

diseases and provide clinically useful information at the large-scale population based screening studies. The results would be helpful for prognosticating disease progression and providing an objective evaluation of cognitive rehabilitation treatments for dementing illness.

Acknowledgment

The work was partly supported by Ministry of Science and Technology, Republic of China, under Grant NSC102-2221-E-182-015-MY3, MOST104-2221-E-182-023-MY2 and Chang Gung Memorial Hospital with Grant No. CMRPD270053, CMRPD2C0041, CMRPD2C0042, CMRPD2C0043.

References

1. Simone Brockman, Binu Jayawardena, Sergio Starkstein. The diagnosis of depression in Alzheimer's disease: review of the current literature. *Neuropsychiatry* 1(4), 377-384 (2011).
2. Seiju Kobayashi, Takao Ishii, Masaru Tateno, et al. The effect of APOE ε4 allele on brain perfusion SPECT in late onset Alzheimer's disease by an automated program, 3DSRT. *Neuropsychiatry* 6(2), 55-63 (2016).
3. Ferri CP, Brayne C. Global prevalence of dementia: a Delphi consensus study. *Lancet. Neurol* 366(9503), 2112-2117 (2005).
4. Lee JD, Yang ST, Wai YY, et al. Probability-based prediction model using multivariate and LVQ-PNN for diagnosing dementia. *Neuropsychiatry* 6(6), 440-450 (2016)
5. Petersen RC. Mild cognitive impairment as a diagnostic entity. *J. Intern. Med* 256(3), 183-194 (2004).
6. Petersen RC, Smith GE, Waring SC, et al. Mild cognitive impairment: clinical characterization and outcome. *Arch. Neurol* 56(3), 303-308 (1999).
7. Nordlund A, Rolstad S, Hellström P, et al. The Goteborg MCI study: mild cognitive impairment is a heterogeneous condition. *J. Neurol. Neurosurg. Psychiatry* 76(11), 1485-1490 (2005).
8. Yaffe K, Petersen RC, Lindquist K, et al. Subtype of mild cognitive impairment and progression to dementia and death. *Dement. Geriatr. Cogn. Disord* 22(4), 312-319 (2006).
9. Huey ED, Manly JJ, Tang MX, et al. Course and etiology of dysexecutive MCI in a community sample. *Alzheimers. Dement* 9(6), 632-639 (2013).
10. Chao LL, Pa J, Duarte A, et al. Patterns of Cerebral Hypoperfusion in Amnesic and Dysexecutive MCI. *Alzheimer. Dis. Assoc. Disord* 23(3), 245-252 (2009).
11. Bookheimer SY, Strojwas MH, Cohen MS, et al. Trail making test A and B: normative data stratified by age and education. *New Eng. J. Med* 343(1), 450-456 (2000).
12. Dickerson BC, Salat DH, Bates JF, et al. Medial temporal lobe function and structure in mild cognitive impairment. *Ann. Neurol* 56(1), 27-35 (2004).
13. Li SJ, Li Z, Wu G, et al. Alzheimer Disease: evaluation of a functional MR imaging index as a marker. *Radiology* 225(1), 253-259 (2002).
14. Minati L, Chan D, Mastropasqua C, et al. Widespread alterations in functional brain network architecture in amnesic mild cognitive impairment. *J. Alzheimers. Dis* 40(1), 213-220 (2014).
15. Teipel SJ, Grothe M, Lista S, et al. Relevance of magnetic resonance imaging for early detection and diagnosis of Alzheimer disease. *Med. Clin. North. Am* 97(3), 399-424 (2013).
16. Fleishera AS, Sherzaid A, Taylor C, et al. Resting-state BOLD networks versus task-associated functional MRI for distinguishing Alzheimer's disease risk groups. *NeuroImage* 47(4), 1678-1690 (2009).
17. Rombouts SA, Barkhof F, Goekoop R, et al. Altered resting state networks in mild cognitive impairment and mild Alzheimer's disease: an fMRI study. *Hum. Brain. Mapp* 26(4), 231-239 (2005).
18. Cordes D, Haughton VM, Arfanakis K, et al. Frequencies contributing to functional connectivity in the cerebral cortex in "resting-state" data. *AJNR. Am. J. Neuroradiol* 22(7), 1326-1333 (2001).
19. Hampson M, Peterson BS, Skudlarski P, et al. Detection of functional connectivity using temporal correlations in MR images. *Hum. Brain. Mapp* 15(4), 247-262 (2002).
20. Peltier SJ, Polk TA, Noll DC. Detecting low-frequency functional connectivity in fMRI using a self-organizing map (SOM) algorithm. *Hum. Brain. Mapp* 20(4), 220-226 (2003).
21. Beckmann CF, DeLuca M, Devlin JT, et al. Investigations into resting-state connectivity using independent component analysis. *Philos. Trans. R. Soc. Lond. B. Biol. Sci* 360(1457), 1001-1013 (2005).
22. Bellec P, Perlberg V, Jbabdi S, et al. Identification of large-scale networks in the brain using fMRI. *NeuroImage* 29(4), 1231-1243 (2006).
23. Damoiseaux JS, Rombouts SA, Barkhof F, et al. Consistent resting-state networks across healthy subjects. *Proc. Natl. Acad. Sci. U S A* 103(37), 13848-13853 (2006).
24. Friston KJ, Frith CD, Liddle PF, et al. Functional connectivity: the principal-component analysis of large data sets. *J. Cereb. Blood. Flow. Metab* 13(1), 05-14 (1993).
25. Peltier SJ, Noll DC. T2* dependence of low frequency functional connectivity. *NeuroImage* 16(4), 985-992 (2002).
26. Wang L, Zang Y, He Y, et al. Changes in hippocampal connectivity in the early stages of Alzheimer's disease: evidence from resting state fMRI. *NeuroImage* 31(2), 496-504 (2006).
27. Greicius MD, Srivastava G, Reiss AL, et al. Default-mode network activity distinguishes Alzheimer's disease from healthy aging: evidence from functional MRI. *Proc. Natl. Acad. Sci. U S A* 101(13), 4637-4642 (2004).
28. Han Y, Wang J, Zhao Z, et al. Frequency-dependent changes in the amplitude of low-frequency fluctuations in amnesic mild cognitive impairment: a resting-state fMRI study. *NeuroImage* 55(1), 287-295 (2011).
29. Amit Y, Geman D. Shape quantization and recognition with randomized trees. *Neural. Comput* 9(7), 1545-1588 (1997).
30. Ho TK. The random subspace method for constructing decision forests. *IEEE. Trans. Patt. Analy. Mach. Intellig* 20(8), 832-844 (1998).
31. Liaw A, Wiener M. Classification and regression by random forest. *R. News* 2(3), 18-22 (2002).
32. Zang TF, Jiang TZ, Lu YL, et al. Regional homogeneity approach to fMRI data analysis. *NeuroImage* 22(1), 394-400 (2004).
33. Ho TK. Random decision forests. *Proc. 3rd Int. Conf. Doc. Anal. Recogn* 1(1), 278-282 (1995).
34. Biseal B, Yetkin FZ, Haughton VM, et al. Functional connectivity in the motor cortex of resting human brain using echo-planar MRI. *Magn. Reson. Med* 34(4), 537-541 (1995).
35. UCL Institute of Neurology, <http://www.fil.ion.ucl.ac.uk/spm/>
36. Talairach J, Tournoux P. Co-Planar Stereotaxic Atlas of the Human Brain: 3-D Proportional System: An Approach to Cerebral Imaging. *Thieme. Classics* (1988).
37. Mazziotta J, A Toga, A Evans, et al. A probabilistic atlas and reference system for the human brain: International Consortium for Brain Mapping (ICBM). *Philos. Trans. R. Soc. Lond. B. Biol. Sci* 356(1412), 1293-1322 (2001).
38. Song XB, Dong ZY, Long XL, et al. REST: A Toolkit for Resting-State Functional Magnetic Resonance Imaging Data Processing. *PLoS. ONE* 6(9), e25031 (2011).
39. Fischl B, Salat DH, Busa E, et al. Whole brain segmentation: automated labeling of neuroanatomical structures in the human brain. *Neuron* 33(3), 341-355 (2002).
40. Breiman L. Random forests. *Mach. Learn* 45(1), 5-32 (2001).